Aerosol and Air Quality Research

ORIGINAL RESEARCH
https://doi.org/10.4209/aaqr.200528

Ground-level Particulate Sulphate and Gaseous Sulphur Dioxide Downwind of an Aluminium Smelter

Dane Blanchard*, **Julian Aherne**

School of the Environment, Trent University, Peterborough, Ontario, K9J 7B8, Canada

ABSTRACT

Particulate sulphate (pSO_4^{2-}) is an atmospheric pollutant known to affect human/environmental health and global radiative-forcing. The Rio Tinto (RT) aluminium smelting facility in Kitimat, British Columbia, is the primary source of sulphur dioxide (SO_2) emissions to the surrounding Kitimat Valley, a relatively isolated and unpolluted region. A network of active two-stage filter-packs and passive-diffusive samplers was established between June 2017 to October 2018 with the objective to evaluate the spatiotemporal variation and relative contribution of pSO_4^{2-} to total anthropogenic atmospheric oxidized sulphur ($SO_x = SO_2 + pSO_4^{2-}$). Average pSO_4^{2-} across all sites (n = 9) was 0.41 µg m^{-3} (24–48 hour exposures) and ranged from 0.03 to 2.03 µg m^{-3}. In contrast, average filter-pack SO_2 ranged from 0.11 to 8.9 µg m^{-3} (during the same exposure periods). The filter-pack pSO_4^{2-}/SO_x concentration ratio (F_s) increased downwind of the smelter, indicating that the relative concentration of pSO_4^{2-} increased with distance from the smelter. Furthermore, the increasing pSO_4^{2-}/vanadium (V) ratio (used as a tracer of smelter emissions) relative to distance confirmed particulate formation was occurring within the emission plume during the sampling period. Irrespective of in-plume aerosol formation, pSO_4^{2-} contributed a relatively minor fraction of total atmospheric SO_x within the emission plume (field campaign averages $F_s < 20\%$; $pSO_4^{2-} < 0.1$ µg S m^{-3}; $SO_2 > 1.0$ µg S m^{-3}).

Keywords: Atmospheric sulphur, British Columbia, Filter-pack, Passive sampler

Received: August 19, 2020
Revised: December 16, 2020
Accepted: December 29, 2020

* **Corresponding Author:**
daneblanchard@trentu.ca

Publisher:
Taiwan Association for Aerosol Research
ISSN: 1680-8584 print
ISSN: 2071-1409 online

1 INTRODUCTION

Anthropogenic emissions of gaseous sulphur dioxide (SO_2) can negatively impact the environment through the deposition of acidic sulphur (S) species, such as sulphuric acid (H_2SO_4) (Parungo *et al.*, 1987). Following release to the atmosphere, SO_2 can undergo several oxidation reactions to form H_2SO_4, which can further condense to become particulate sulphate (pSO_4^{2-}) (Friedlander, 1978; Huntzicker *et al.*, 1984). These particulates (also referred to as aerosol sulphate) are of unique concern owing to their longevity in the atmosphere and potential impact to environmental and human health (Davidson *et al.*, 2005; Hains *et al.*, 2008; Lee *et al.*, 2011). Aerosol SO_4^{2-} can dominate total fine particulate matter ($PM_{2.5}$), particularly in regions downwind of significant SO_2 emissions sources (Husar *et al.*, 1976; Hand *et al.*, 2012), and is responsible for a large fraction of global tropospheric non-sea-salt sulphate (nss-pSO_4^{2-}) (Husar *et al.*, 1976). From hereon, nss-pSO_4^{2-} will be referred to as pSO_4^{2-} unless otherwise stated. Particulate SO_4^{2-} can act as cloud condensation nuclei that encourage the production of dense, highly reflective clouds, which in addition to the direct back-scattering of light by pSO_4^{2-}, can alter planetary albedo (Wigley, 1989; Solomon *et al.*, 2007). Furthermore, pSO_4^{2-} can contribute to acidic deposition via processes of wet and dry removal (Nicholson and Davies, 1987).

The oxidation of SO_2 can occur through two broad reaction categories, defined as the gas and liquid phase reaction pathways (Gorham, 1955). The most significant gas-phase reaction pathway involves the oxidation of SO_2 by the hydroxyl radical (OH^-) (Bunce, 1998). In the absence of additional reactions to inhibit the production of OH^-, the reaction becomes SO_2-limited (Margitan, 1984; Mohnen, 1988). Previous studies have employed a S concentration ratio (F_s) to evaluate in-atmosphere oxidation of SO_2 (Grosjean and Friedlander, 1975; Kadowaki, 1986; Khoder, 2002). The ratio indicates the fraction of pSO_4^{2-} relative to the total combined concentration of SO_x species (SO_2 and pSO_4^{2-}). The ratio can provide insight on the distribution of particulate and gaseous S species, especially when paired with additional environmental variables, which can reveal the underlying factors influencing pSO_4^{2-} formation (Khoder, 2002). Active filter-packs have been widely used to evaluate pSO_4^{2-} spatial and temporal variability, particularly in relation to SO_2 conversion (Luria *et al.*, 2001; Khoder, 2002; Watanabe, 2006). Further, previous studies investigating in-plume SO_2 oxidation have employed additional pollutant species (known to be associated with the emission source) as tracers for point-source emissions. Roberts and Williams (1979) used particulate lead (Pb) as a tracer for emissions produced from a sulphide smelter in remote Australia, further referring to the ratios of pSO_4^{2-} and Pb as an indicator of in-plume pSO_4^{2-} formation via oxidization.

In 2015, the Rio Tinto (RT) aluminium (Al) smelter situated in Kitimat, British Columbia, completed major developments to improve production output and efficiency. The "Kitimat Modernization Project" (KMP), included a permitted increase of facility SO_2 emissions (a known by-product of Al smelting). Smelter emissions are released into the Kitimat Valley, a remote northern western region, which excluding the RT facility (and downwind regions), experiences low background levels of anthropogenic pollution (Williston *et al.*, 2016). Prior to the completion of the KMP, an extensive environmental assessment (the Sulphur Dioxide Technical Assessment Report, or STAR) employing dispersion modelling techniques was conducted in-part to evaluate the dispersion of SO_2 throughout the surrounding region (ESSA technologies Ltd., 2013). Despite these efforts, ambient pSO_4^{2-} was not monitored within the Kitimat Valley, leaving many uncertainties regarding the spatial and temporal variability of secondary-sulphate aerosols downwind of the smelter. The Al smelting process releases trace vanadium (V) emissions, which following the combustion of contaminated petroleum coke is released as fine (< 2.5 µm) and/or ultrafine (< 0.01 µm diameter) vanadium pentoxide (V_2O_5) particulates, a water-soluble species (Nriagu, 1998; Espinosa *et al.*, 2001; Singh *et al.*, 2002; Jha *et al.*, 2012; Edwards, 2014; Schlesinger *et al.*, 2017).

Between June 2017 to June 2018, active filter-pack and passive diffusive samplers were deployed during four field campaigns to simultaneously evaluate the variation of SO_2 and pSO_4^{2-} throughout the Kitimat region, using F_s to assess the relative concentrations of SO_x species. Previous biomonitoring campaigns conducted by Cowden and Aherne (2019) identified RT as a source of V emissions; as such, atmospheric V was included in the current study as tracer of smelter emissions. The primary objectives of this research were to evaluate the spatial and temporal variation of aerosol sulphate in the Kitimat Valley, confirm whether smelter SO_2 emissions contribute to downwind formation of pSO_4^{2-}, and to determine the relative contribution of pSO_4^{2-} to total ambient SO_x in the study region.

2 METHODS

2.1 Study Region

The RT smelting facility is situated several kilometers south-west of the municipality of Kitimat, BC. This small township (population ~8,000) is located at the northern limit of the Douglas Channel, which extends ~90 km inland from the Pacific Ocean through the Skeena provincial region. The Kitimat Valley expands northward from the channel's end, encompassing the municipalities of Kitimat, Kitimaat Village (< 10 km south of Kitimat) and Terrace (~50 km to the north of Kitimat), as seen in Fig. 1. The valley has an internal surface area of ~3000 km^2 and a maximum width of 15 km (Clague, 1985). As a result of past and ongoing activities associated with the forestry industry, large sections of the valley have been subject to deforestation and subsequent re-planting activities (Clague, 1994).

Kitimat experiences a relatively wet and temperate climate owing to its proximity to the Pacific Ocean. Based on the 30-year climate normal (1981–2010), average annual temperature in Kitimat was 7.4°C, ranging from –1.7°C in January to 16.7°C in July. Normal total annual precipitation was 2211 mm, with the greatest volume falling during the autumn months (324 mm, October),

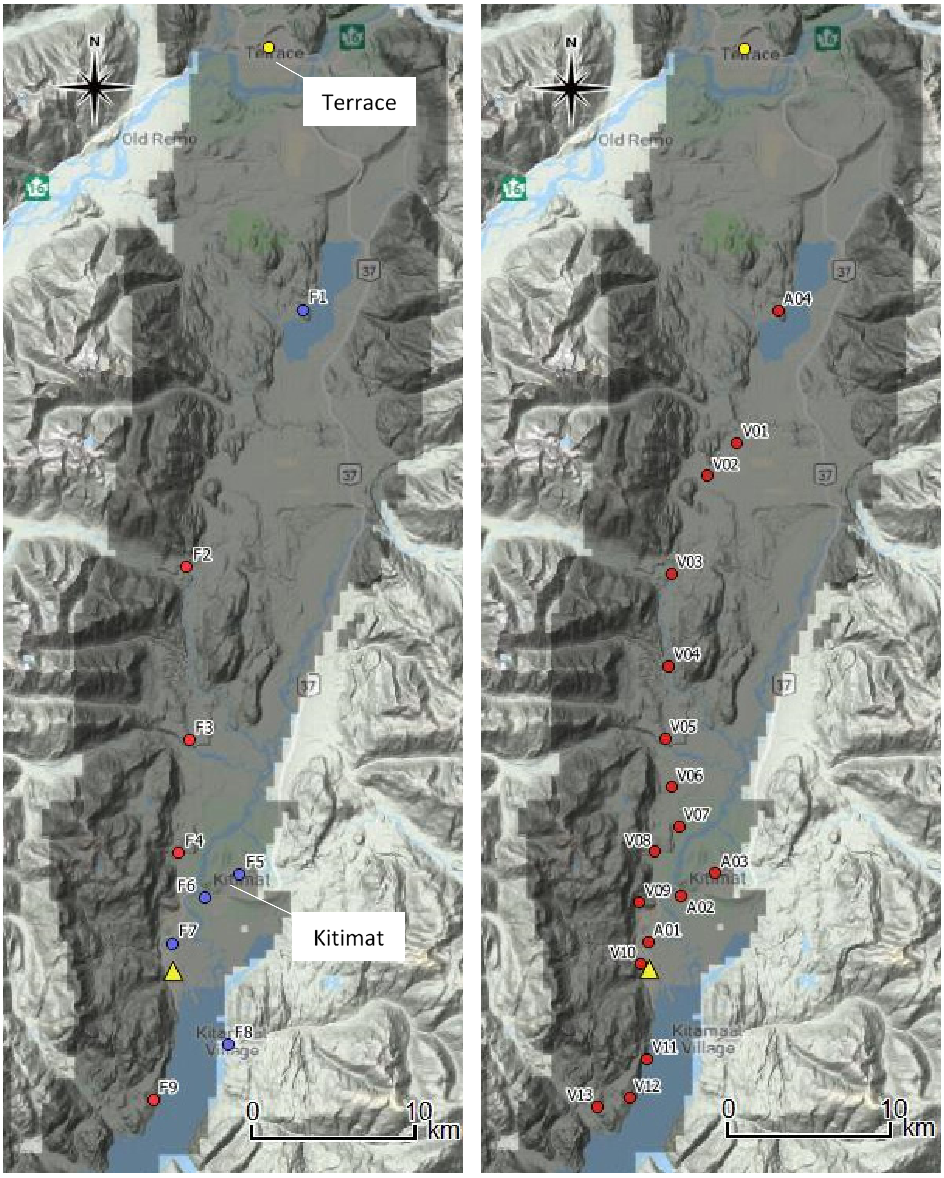

Fig. 1. Overview of the (left) active filter-pack and (right) SO_2 passive sampling locations established throughout the Kitimat Valley. Filter-pack sites co-located at monitoring stations are indicated by the blue-filled circles, while sites which received portable sampler deployments are displayed as red-filled circles. Filter-pack sites have been labelled with a site ID with is preceded with an "F" (Table 1). Passive sampler sites (IVL) established at active monitoring stations or independently along the valley are indicated by labels preceded by "A" and "V" respectively (Table 1). The yellow-filled triangle and circle symbols indicate the location of the RT smelting facility and the Terrace Middle School air-quality monitoring station, respectively. The shaded map-region represents the area within which average modelled annual SO_2 exceeded 1.5 $\mu g\ m^{-3}$ at ground-level during the post-KMP scenario (ESSA Technologies Ltd., 2013).

and the lowest during the summer (62 mm, July) (Environment and Climate Change Canada, 2017). Air currents originating from inland BC or the Pacific are forced by the prominent topography of the surrounding region, steering predominant winds north or south along the Kitimat Valley. Owing to the relative consistency of these wind patterns, pollutant dispersion often occurs within a well-defined plume extending north or south from the RT facility along the western wall of the Kitimat valley, as shown in Fig. 1. Regions falling within the well-defined plume path experience dramatically different air quality (higher concentration of SO_2) compared to locations immediately outside the plume (ESSA Technologies Ltd., 2013).

2.2 Sampling Campaigns and Sites

Between June 2017 and June 2018, filter-pack samplers were deployed during four field campaigns in the Kitimat Valley. Exposure periods generally lasted 1–2 weeks, during which the active samplers operated semi-continuously. The filter-pack network consisted of nine sampling locations, of which sites F1, F2, F3, F4, F7, and F9 (displayed in Fig. 1 and Table 1) were positioned along the central transect within the plume path, the remaining locations (F5, F6, and F8) were established outside the plume path. Further, the filter-pack samplers were deployed at existing atmospheric monitoring stations, including Lakelse Lake (F1), Whitesail (F5), Riverlodge (F6), Haul Road (F7), and Haisla (F8), so that additional monitoring data could be obtained for a range of pollutant and meteorological variables, including continuous UV-fluorescence measurements of ambient SO_2 (with exception of Lakeslse Lake).

A total of nine filter-pack exposures were collected during the first field campaign (June 11–21, 2017), increasing to 20 and 21 during the second (October 21–27, 2017) and third (February 16–23, 2018) sessions, respectively. Owing to limited site accessibility during the first three sampling periods, filter-pack samplers were exclusively co-located at existing monitoring stations for 24 h exposures, see Fig. 1 and Table 1. The exposures occurred back-to-back and simultaneously between stations with exception of the first campaign, where one sampler was re-located to a new station every third day. During the fourth, sampling period (June 13–July 6, 2018), 41 exposures were collected across eight sampling locations extending north and south along the valley, as shown in Fig. 1 and Table 1. Exposures were extended to 48 h, generally running back-to-back and simultaneously between stations. Passive-diffusive SO_2 samplers, supplied by the Swedish Environmental Research Institute "IVL" (URL: diffusivesampling.ivl.se) were deployed throughout the Kitimat Valley as back-to-back monthly exposures between June–October of both 2017 and 2018. The IVL SO_2 samplers have been widely used globally (Ferm and Rodhe, 1997; Carmichael *et al.*, 2003). These samplers are well represented in the peer-review literature and have been shown to have good correspondence with continuous samplers (Ferm and Rodhe, 1997, Swaans *et al.*, 2007). In the current study, passive samplers were routinely deployed at seventeen sites throughout the Kitimat Valley. All but two IVL sites (A02 and A03) were established along the transect on the valley floor, providing coverage of the emission plume extending north and south of the RT smelter. Furthermore, eight of the sampling sites (A04, V03, V05, V08, A03, A02, A01, and V12) were co-located with active filter-pack samplers (see Table 1).

2.3 Active Filter-pack Samplers

Gaseous SO_2 and pSO_4^{2-} were simultaneously measured via a two-stage filter-pack cartridge, where an in-line pump system enabled active sampling of the ambient atmosphere. The filter-pack cartages designed by the Norwegian Institute for Air Research (NILU; www.nilu.no) consisted of three threaded compartments which housed two filter papers upon assembly. The outer-most

Table 1. Description of filter-pack sampling locations including site name and corresponding Map ID (see Fig. 1), coordinates (latitude and longitude), and elevation (m). Details regarding the number of exposures conducted at each site during each respective field campaign are provided under the "Field Campaign" columns.

Map ID[a]	Site Name	Latitude	Longitude	Elevation (m)	Field Campaign				
					1	2	3	4	Sum
F1	A04 (Lakelse Lake)	54.37730	–128.57756	111	3	5	5	8	21
F2	V03	54.23598	–128.68712	127	-	-	-	4	4
F3	V05	54.14080	–128.68590	114	-	-	-	7	7
F4	V08	54.07863	–128.69545	68	-	-	-	7	7
F5	A03 (Whitesail)	54.06690	–128.63910	94	-	6	6	-	6
F6	A02 (Riverlodge)	54.05397	–128.67101	18	3	6	6	4	19
F7	A01 (Haul Road)	54.02927	–128.70190	11	3	3	4	5	15
F8	A00 (Haisla Village)	53.97323	–128.65077	5	-	-	-	3	3
F9	V12	53.94320	–128.72061	114	-	-	-	3	3
					Total Exposures = 85				

[a] Map ID refers to the labels displayed in Fig. 1.

stage housed a Whatman 40 cellulous filter (47 mm diameter, 8.0 µm pore size) designated to collect pSO_4^{2-} and additional particulate matter (PM) species (Arends *et al.*, 1997), the inner-stage collected gaseous SO_2 on a second Whatman 40 filter, which had been pre-treated with an alkaline solution of potassium hydroxide (KOH). Methods including sampler preparation, deployment, and analysis followed those outlined in the EMEP Manual for Sampling and Analysis (EMEP, 2001). The first stage filters did not require laboratory preparation, while the Whatman 40 filters in the second stage were individually pre-treated with 300 µL of alkaline impregnation solution (1.0 M KOH/10.0% glycerol in methanol). Filter preparation was performed within a sealed glove box, which was continually pressurised with SO_2-filtered air (using the KOH solution as the filtering agent). Filter media were individually triple sealed in plastic Ziploc® bags during transport and storage periods. In the field, samplers were attached in-line to a vacuum pump (operating at 15 L min^{-1} during field campaigns one to three and 7.5 L min^{-1} during campaign four) and flow meter (flow rates recorded at the start and end of each exposure); filter-packs were housed at the end of a PVC rain shelter, refer to Fig. 2 and Fig. S1.

Five pSO_4^{2-} and SO_2 filter-media blanks were included during sampling periods one to three, while twelve pSO_4^{2-} and ten SO_2 filter blanks were included during the final campaign. In an effort to evaluate sampler variation, duplicate active filter-pack systems were co-deployed at sampling sites during four exposures. Sampler blanks where used to determine analyte detection limits, which where calculated as: standard deviation [n blanks] × t-value 99.0% confidence critical value.

First stage filters were extracted in 15 mL conical tubes filled with 10 mL deionized water. Samples were inverted three times, then placed in an ultrasonic bath for 30 minutes prior to further analysis. Within a filtered glovebox, second stage filters were placed into 15 mL conical tubes filled with 10 mL of 0.3% hydrogen peroxide (H_2O_2) deionized water solution, after which samples were inverted several times and left for an hour. Using a 20 ml plastic syringe and 0.45 µm pore-size syringe filter, both extraction solutions were removed from their respective conical tubes and placed into 0.5 mL vials. Samples were analysed for inorganic anion species via ion chromatography (IC). Following Zbieranowski and Aherne (2012), a 1 mL aliquot of extraction solution from the uncoated filter membrane was analysed for ammonium (NH_4^+) via colourmetric analysis (analysis was conducted during the final sampling period only); however, samplers reported concentrations uniformly below detection limit. Finally, the remaining aerosol extraction solution was filtered (0.45 µm syringe filters) and acidified (2% HNO_3) for determination of water-soluble elements (specifically V) via inductively coupled plasma mass spectroscopy (ICP-MS). Prior to each field campaign all components of the filter-pack cartridge were individually rinsed in reverse osmosis (RO) water and subsequently placed in a bath of oxalic acid for 12 hours, after which the sampler parts were rinsed in B-Pure lab water. In the field, the filter-pack cartridges were soaked in baths of RO water between exposures. To control for potential filter contamination between exposures, field blanks were loaded into (as if to collect a sample) and subsequently removed from select washed cartridges.

Fig. 2 and Fig. S1. detail the two filter-pack sampler models developed during the study. The first system utilized a powerful laboratory-grade diaphragm pump capable of operating at a flow

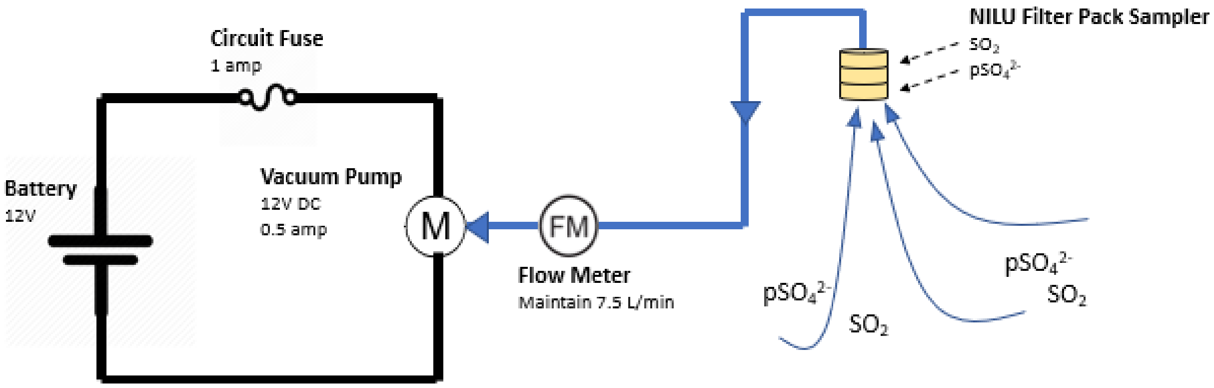

Fig. 2. Diagram displaying the layout and components of the battery powered filter-pack system. Note the non-portable sampler system is identical in design with exception of the lab-pump and power source (AC electrical outlet).

rate of 15 L min^{-1}. The lab-grade pumps could only be deployed in locations with immediate access to AC electrical outlets, therefore the filter-pack sampling systems were co-deployed at active monitoring stations (see Fig. 1 and Table 1 for site locations). In contrast, at sites without an AC power source, a portable active sampler fitted with a low-amperage (0.5 amp), direct current (DC) diaphragm pump was deployed. The low-amperage pump powered by a single 12 V battery was capable of operating at a flow rate of 7.5 L min^{-1} for extended periods. Portable filter-pack exposures were extended to 48 h to compensate for the reduced flow rate. Filter-packs deployed at existing active monitoring stations were located ~4–5 m above ground level, while the portable sampler air intakes were deployed ~1 m above ground level. Active sampling systems were tested for leaks during each exposure by covering the air-intake (without the filter-pack attached) with an open hand.

Ambient concentrations of aerosol and gaseous species measured by the filter-pack sampler were determined by the following equation (EANET, 2003):

$$C_{air} = net\ C_{sol} \times V_{sol}/V_{air} \tag{1}$$

where C_{air} is the ambient analyte concentration (µg m^{-3}), net C_{sol} is the net analyte concentration of the solution (mg L^{-1}), V_{sol} is the volume of solution used (ml), V_{air} is the volume of air sampled – corrected at 20°C, 1 atm (m^3). Net C_{sol} was calculated by the following (EANET, 2003):

$$net\ C_{sol} = C_{sol,sample} - C_{sol,blank} \tag{2}$$

where $C_{sol,sample}$ is the concentration of solution extracted from the SO_2 or pSO_4^{2-} filters, and $C_{sol,\mathrm{blank}}$ is the concentration of solution extracted from blank filter papers. The observed atmospheric sulphate originating from sea-spray was subtracted from the total observed pSO_4^{2-} to determine the non-sea-salt SO_4^{2-} fraction (nss-pSO_4^{2-}). The sampler adjustment was calculated based on the sea-salt chloride (Cl^-) to sulphate (mg L^{-1}) ratio of 0.14 (Millero, 1974):

$$[\text{nss-pSO}_4^{2-}] = [\text{pSO}_4^{2-}] - 0.14[\text{pCl}^-] \tag{3}$$

where [nss-pSO_4^{2-}], [pSO_4^{2-}], and [pCl^-] is the average extraction concentration (µg L^{-1}) of the respective particulate species in the extractant sample. Particulate chloride was collected on the first stage of the filter-pack and analysed via IC. The sulphur concentration ratio (F_s) was calculated following Grosjean and Friedlander (1975) and Khoder (2002):

$$F_s = \frac{\left[\text{nss-pSO}_4^{2-}\right]}{\left[\text{SO}_2\right] + \left[\text{nss-pSO}_4^{2-}\right]} \tag{4}$$

where [nss-pSO_4^{2-}] is the sea-salt corrected particulate sulphate concentration, expressed as SO_2 (µg m^{-3}), and [SO_2] is the average gaseous SO_2 concentration (µg m^{-3}).

2.4 Passive-diffusive Sampling

Passive-diffusive SO_2 samplers manufactured by IVL have been widely used for air quality research (Carmichael *et al.*, 1995; Ferm and Svanberg, 1998; Zhang *et al.*, 2014). Samplers were received from IVL in sealed plastic cylindrical containers, during deployment they were removed and attached to the underside of a rain shelter via metal clamp, as shown in Fig. S2. Upon retrieval, samplers were stored in their original plastic containers to be shipped back to IVL for analysis. One IVL field blank was included with each exposure, while a total of 35 duplicate samplers were deployed in the field throughout the study.

2.5 Evaluation of Sampler Accuracy

Active filter-pack and passive-diffusive samplers were co-deployed at ambient air quality monitoring stations throughout the study period, as shown in Table 1. The monitoring stations provided continuous SO_2 data (measured by UV fluorescence) that were compared against corresponding passive sampler and filter-pack observations. Agreement between samplers was evaluated via linear regression analysis, Wilcoxon signed rank test, and determination of sampler bias. The measured percent coefficient of variation (CV) between replicate samplers was applied to evaluate sampler precision.

2.6 CALPUFF Dispersion Model

The atmospheric dispersion model, CALPUFF, was employed during the STAR investigation (independent from the present study) to simulate atmospheric SO_2 throughout the Kitimat Valley (ESSA Technologies Ltd., 2013). The model was configured by Trinity Consultants (www.trinityconsultants.com) to predict plume dispersion, atmospheric chemical conversions, and wet/dry pollutant removal processes. It was determined that CALPUFF was an appropriate model to simulate plume dispersion in the Kitimat Valley largely owing to the model's ability to estimate long range transport ($>$ 50 km), simulate plume transport over complex terrain (Kitimat valley and surrounding mountains), and represent buoyant plume rise from line emission sources, such as rooftop vents (ESSA Technologies Ltd., 2013).

Three years of regional meteorological observations (2006, 2008, and 2009) measured at surface, upper air, and National Oceanic and Atmosphere Administration (NOAA) buoy stations were compiled for the simulation and deemed representative of long-term meteorology (ESSA Technologies Ltd., 2013). Further, the MESOPUFF chemical transformation algorithms were employed to simulate the reactivity of several pollutant species (including SO_2) throughout the modelled airshed. Details regarding model parameterization and QA/QC can be found in ESSA Technologies Ltd. (2013).

The resulting model predicted atmospheric dispersion and deposition under both pre- and post-KMP emission scenarios, assuming the smelter released SO_2 at the maximum permitted emission rates of 27 and 42 tonnes per day ($t\ d^{-1}$), respectively. The model produced estimated hourly SO_2 ($\mu g\ m^{-3}$) on a 500 m × 500 m spatial grid throughout the study region, which was subsequently consolidated into annual averages (ESSA Technologies Ltd., 2013). In the current study, these existing CALPUFF simulations were used to extrapolate observed pSO_4^{2-} to the entire valley.

2.7 Data Analysis

Filter-pack and passive-diffusive sampler data were both not normally distributed, as independent Shapiro-Wilk tests (for all available sampler datasets) rejected the null hypothesis ($p > 0.05$). Assuming non-normality, non-parametric tests were exclusively employed for statistical analysis.

Average metrological data during the June 2017–July 2018 study period was obtained from the Whitesail monitoring station (Table 1), where hourly temperature (°C), relative humidity (%), wind speed ($m\ s^{-1}$), and wind direction (°deg; anemometer located 10 m above ground-level) were recorded. Hourly wind direction data were transformed according to the difference between the reported value (degrees) and 180 degrees. The transformed data fit a linear scale, where decreasing values approached southerly winds and higher values approached northern winds. The combined meteorological data was tabulated to assess average values during each of the four sampling campaigns, wind-rose analysis (using non-transformed data) was also plotted for each period. Monthly daily-average SO_2 emissions data ($t\ d^{-1}$) from the RT smelting facility were evaluated against ambient SO_x variability within the study region.

Filter-pack observations were initially assessed to determine general spatial and temporal trends throughout the Kitimat Valley during the study period. Principal component analysis (PCA) was applied to evaluate the underlying variance of the combined pollutant (SO_2, particulate ions, and water-soluble trace elements), geographic location (elevation [Elev] and distance from smelter [Dist]), and corresponding metrological data (temperature [T], wind speed [WS], wind direction [WD], relative humidity [RH]) associated with the filter-pack network. Data from exposure four only was evaluated via PCA, as previous exposures presented an insufficient number of observations to produce meaningful output.

Bivariate analysis was employed to evaluate the potential correlation between meteorological and pollutant variables. Correlation analysis was conducted via a Spearman's Rank-Order non-parametric test; the null hypothesis of which states that the Spearman correlation coefficient, "rho" (ρ) between paired variables is equal to zero. Only significant correlations, as determined by the Spearman's test ($p > 0.05$), were reported (unless stated otherwise).

The observed curve of best fit between filter-pack estimated SO_2 and F_s was employed as a function to extrapolate F_s from the SO_2 observed via the IVL passive sampler network (see Fig. 1) and the 500 m × 500 m grid of annual average SO_2 simulated by the CALPUFF dispersion model (ESSA Technologies Ltd., 2013). Following estimation of F_s, the corresponding concentration of pSO_4^{2-} was derived via rearrangement of Eq. (4):

$$\left[pSO_4^{\;2-}\right] = \frac{F_s \times \left[SO_2\right]}{1 - F_s} \times 1.50 \tag{5}$$

where $[pSO_4^{2-}]$ is the ambient concentration of pSO_4^{2-} ($\mu g\ m^{-3}$), and 1.50 is the conversion constant (molar fraction) from pSO_4^{2-} expressed as SO_2 to SO_4^{2-} ($\mu g\ m^{-3}$).

Following Roberts and Williams (1979), filter-pack measured V was used a tracer for smelter emissions within the study region. Furthermore, the filter-pack tracer species was evaluated during each exposure as a ratio of $[pSO_4^{2-}]/[V]$, which were individually recorded as $\mu g\ m^{-3}$, and ng m^{-3}. Given its low dry deposition velocity similar to pSO_4^{2-} (Hazi *et al.*, 2003; Sakata and Marumoto, 2004), the V ratio served as an alternative metric to F_s.

3 RESULTS

3.1 Regional Summary

The highest average temperature during the study was recorded in July of 2018 (20.3°C), while the lowest occurred in February 2018 (–2.7°C). Monthly average wind speed experienced moderate variation throughout the study period (CV = 19%); Table S1 (supporting information), Table 2, and Fig. 3 illustrate that wind speeds were the strongest and most southerly during the first (June 2017) and fourth sampling period while winds during the second (October 2017) and third campaigns were comparatively weak and northerly. In-contrast, RH was observed to be highest during the winter, and lowest during the summer. Average wind direction experienced high monthly variation (CV = 90%); spring/summer winds blew predominantly from the south while winter/autumn months experienced northerly winds.

As shown in Fig. 4, monthly-average smelter SO_2 emissions (t d^{-1}) were reported at their highest during the summer and early-autumn months (June–September) of 2017 (ranging from 31.0 to 32.9 t d^{-1}), later declining throughout September 2017 to March 2018 (ranging from 22.2 to 28.5 t d^{-1}).

3.2 Evaluation of Sampler Performance

Average method detection limits for filter-pack analytes was 0.03 $\mu g\ m^{-3}$ (pSO_4^{2-}), 0.12 $\mu g\ m^{-3}$ (SO_2), 0.03 ng m^{-3} (V), and 0.20 $\mu g\ m^{-3}$ (Cl^-) across the full study period. Filter-packs experienced low inter-sampler variation (high precision), as co-deployed replicate samples presented a CV of 5% and 4% for sampled pSO_4^{2-} and SO_2, respectively. A strong linear correlation between filter-pack and monitoring station measured SO_2 ($R^2 = 0.64$) was observed over the four sampling periods, as seen in Fig. 5. However, the filter-pack samplers presented an average bias error of + 70%, as the samplers expressed a tendency to over-estimate SO_2 at low-ambient concentrations ($< 0.5\ \mu g\ m^{-3}$) (Wilcoxon signed rank test [$p < 0.05$]). Comparison of filter-pack observations above 0.5 $\mu g\ m^{-3}$ (measured by continuous samplers) resulted in an average bias of –44%.

Table 2. Summary of average temperature (°C), wind speed (m s^{-1}), relative humidity (%), and wind direction (°deg) observed at Whitesail monitoring station during individual periods. Exposure start and end dates are displayed.

Sampling Period	Start (M/D/Y)	End (M/D/Y)	Temperature (°C)	Wind Speed (m s^{-1})	Wind Direction (°deg)	Relative Humidity (%)
1	6/11/2017	6/21/2017	14.3	3.5	44.0	72.4
2	10/21/2017	10/27/2017	6.7	2.5	113.3	90.3
3	2/16/2018	2/23/2018	–4.4	2.9	136.6	73.4
4	6/13/2018	7/6/2018	16.6	3.5	54.4	69.3

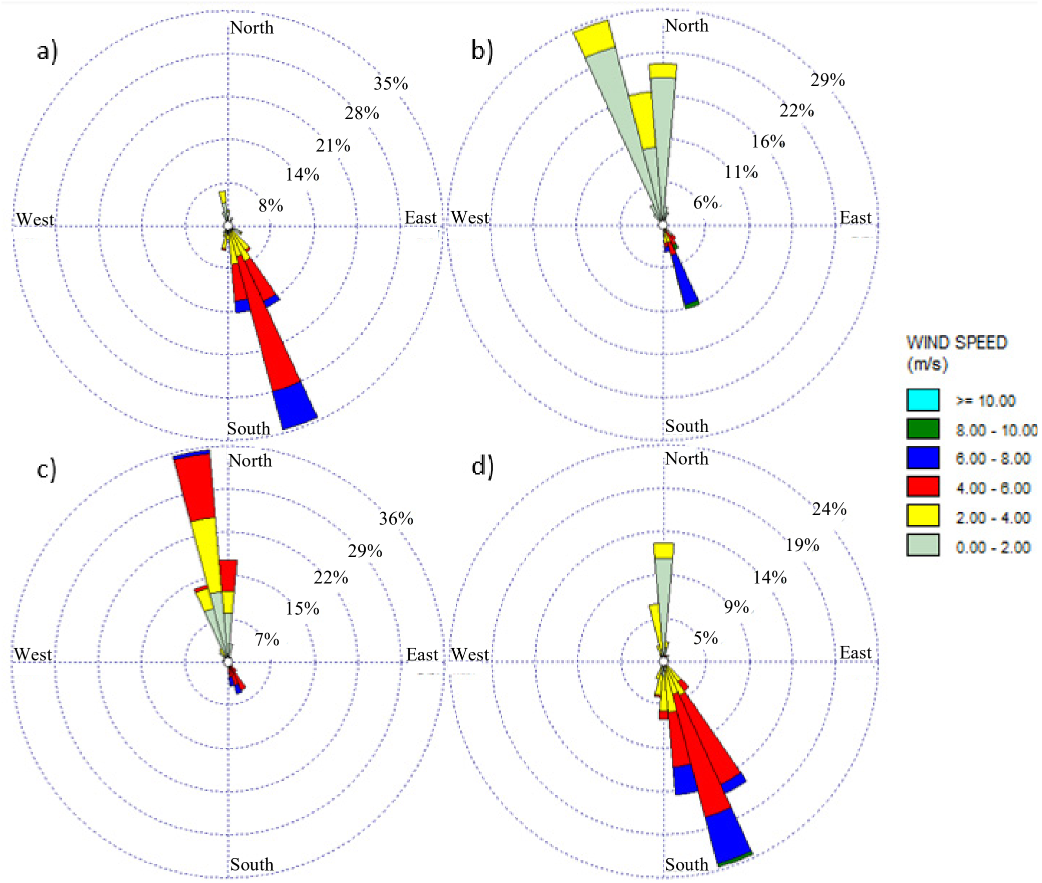

Fig. 3. Wind rose plots displaying hourly recorded wind direction (cardinal) and speed (m s^{-1}) frequencies (measured at Whitesail station) during field campaigns (a) one (June 2017), (b) two (October 2017), (c) three (February 2018), and (d) four (June–July 2018).

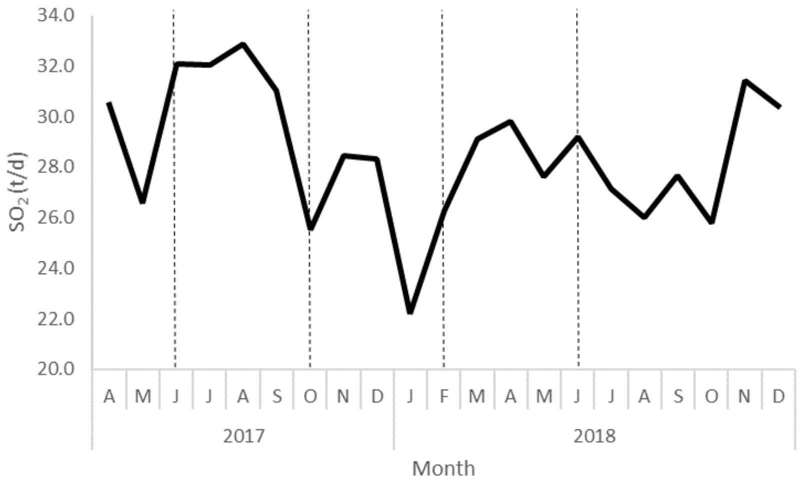

Fig. 4. Average monthly SO_2 emissions (t d^{-1}) from the RT aluminium smelting facility between April 2017 to December 2018. The dashed-vertical lines highlight the individual filter-pack exposure periods (one to four) throughout the study period (June 2017–October 2018).

IVL passive-diffusive samplers displayed low inter-sampler variation as replicate samplers deployed throughout the study period presented an average CV of 6%. Comparison of active monitoring against co-deployed passive sampler observations (collected throughout the study period) revealed a relatively strong agreement between instruments ($R^2 = 0.87$) (Wilcoxon signed

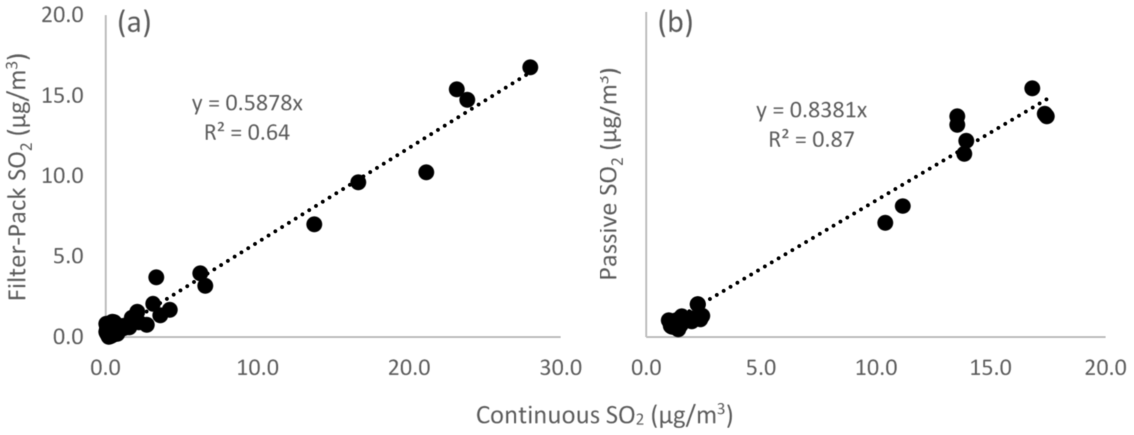

Fig. 5. Comparison of ambient SO_2 (µg m^{-3}) measured by monitoring station continuous samplers against co-deployed a) filter-pack samplers and b) IVL passive samplers throughout the study period. The line of best fit with corresponding regression-equation and coefficient of determination are displayed for each figure.

rank test [$p < 0.05$]). The passive samplers displayed an average negative bias of –27% over the study period.

3.3 Filter-pack Observations

As displayed in Table 3, average observed pSO_4^{2-} at Haul Rd. (F7), Riverlodge (F6), and Lakelse Lake (F1) stations ranged from 0.15 to 0.24 µg m^{-3}, 0.03 to 0.34 µg m^{-3}, 0.41 to 2.03 µg m^{-3}, and 0.17 to 0.49 µg m^{-3} during field campaigns one to four, respectively. Among the three monitoring stations, pSO_4^{2-} was highest at Haul Road during exposures one, two, and four, and highest at Lakelse Lake during the third sampling period. Average SO_2 ranged from 0.72 to 8.90 µg m^{-3}, 0.19 to 5.25 µg m^{-3}, 0.11 to 7.40 µg m^{-3}, and 0.91 to 8.23 µg m^{-3} during exposures one through four respectively. Exposure-average SO_2 was highest at Haul Road and lowest at Lakelse station throughout the study period (with exception of exposure four, where Riverlodge experienced the lowest concentrations). Average estimated F_s ranged from 3.3 to 16.5%, 13.3 to 21.2%, 16.0 to 58.0%, and 5.2 to 12.7% during campaigns one through four, respectively. With exception of the third field campaign, Lakelse experienced significantly higher F_s (Wilcoxon, $p < 0.05$) than Haul Road, as displayed in Table 3. Filter-pack pCl^-ranged between 0.07 to 0.48 µg m^{-3}; pCl^- fell below detection limits during the second field campaign, a period which coincided with predominantly northly winds. Site-average V ranged from 0.01 to 2.82 ng m^{-3}.

Average SO_2 and V during separate field campaigns (excluding the third period) were frequently significantly higher (Wilcoxon, $p < 0.05$) at locations along the central plume transect compared with sites located outside the plume (including sites F5, F6, and F8). Lakelse Lake was an exception to this trend, as average concentrations showed no significant difference, or were lower than other background sites (except during the winter period). Furthermore, sites established downwind (north) of the facility (F7 and F1) consistently presented higher average SO_2 and V nearest to the smelter (F7). Continuing this trend, filter-pack measured pSO_4^{2-}, SO_2, and V during the fourth exposure decline in concentration with distance from the RT smelter, as seen in Fig. 6. Aerosol sulphate appeared to initially increase within the first ~13 km of the smelter, after which concentrations rapidly declined; this observed decline was driven by Lakelse station data. Fig. 6 shows that estimated F_s and pSO_4^{2-}/V ratios increased with distance from the smelter (both presenting an $R^2 = 1.0$). Additional sites in proximity to the smelter but outside the plume's central transect (F8, F6, and F5) reported significantly lower pSO_4^{2-}, SO_2, and particulate V relative to sites located within the plume (F7, F4, F3, etc.), as determined by Wilcoxon Signed Rank test ($p < 0.05$). In contrast, the corresponding F_s values were notably larger at sites removed from the emission plume compared to observations downwind of the smelter, as shown in Table 3.

3.4 Filter-pack Covariance

Initial evaluation using PCA of combined filter-pack, meteorological, and site-specific data from

Table 3. Average measured pSO_4^{2-} ($\mu g\ m^{-3}$), F_s (%), SO_2 ($\mu g\ m^{-3}$), and V (ng m^{-3}), during respective field campaigns one through four at each filter-pack sampling site. See Fig. 1 for site locations. Individual sampling period averages are displayed.

	Field Campaign (1–4)							
	1^{a}	2^{b}	3^{c}	4^{d}	1^{a}	2^{b}	3^{c}	4^{d}
Site ID	pSO_4^{2-} ($\mu g\ m^{-3}$)				SO_2 ($\mu g\ m^{-3}$)			
F1^{f}	0.15	0.03	2.03	0.17	0.72	0.19	0.11	1.11
F2	-	-	-	0.54	-	-	-	4.4
F3	-	-	-	0.58	-	-	-	4.97
F4	-	-	-	0.47	-	-	-	6.47
F5^{g}	-	0.14	0.4	-	-	0.36	0.32	-
F6^{h}	0.17	0.19	0.41	0.17	1.01	0.67	0.53	0.91
F7^{i}	0.24	0.34	0.68	0.49	8.9	5.25	7.4	8.23
F8^{j}	-	-	-	0.14	-	-	-	0.57
F9	-	-	-	0.51	-	-	-	2.61
Average^{e}	0.22	0.19	1.1	0.29	3.54	2.04	2.68	3.42
	F_s (%)				V (ng m^{-3})			
F1^{f}	16.5	13.3	58.0	10.4	0.26	0.0	0.06	0.28
F2	-	-	-	7.4	-	-	-	1.49
F3	-	-	-	7.1	-	-	-	1.45
F4	-	-	-	5.7	-	-	-	2.55
F5^{g}	-	29.2	39.8	-	-	0.0	0.08	-
F6^{h}	14.6	21.0	32.4	12.7	0.22	0.01	0.16	0.39
F7^{i}	3.3	21.2	16.0	5.2	0.22	0.02	1.90	2.82
F8^{j}		-	-	17.7	-	-	-	0.09
F9	-	-	-	15.2	-	-	-	2.13
Average^{e}	11.5	18.5	35.5	9.4	0.24	0.01	0.55	1.40

[a] June 2017; [b] October 2017; [c] February 2018; [d] June–July 2018; [e] Values presented in the row "Average" represent the combined exposure average between sites Haul Rd (F7), Riverlodge (F6), and Lakelse (F1) stations; [f] Lakelse Station; [g] Whitesail station; [h] Riverlodge station; [i] Haul Road station; [j] Kitimaat Village station.

the fourth sampling period revealed two principal components (PC) responsible for 59.4% of total observed variance. Fig. 7 shows that the PC1 (responsible for 41.9% of observed variation) was largely influenced by Li, Na, Mg, Al, Si, Mn, Fe, and F, all of which decreased with distance from smelter (Dist) and elevation (Elev); this PC may have been representative of dust emissions from the RT facility and unpaved access roads. As seen in Table S2, the above-mentioned particulate variables were strongly correlated with one another, and uniformly displayed negative correlations with elevation and distance from the smelter. PC2 (responsible for 17.5% variance) was characterized by V, pSO_4^{2-}, SO_2, RH, and WS, which inversely covaried with F_s, T, and WD. The second PC may have represented the S-enriched smelter plume, considering the covariance between V and S species. As seen in Table S2, filter-pack variables V, pSO_4^{2-}, and SO_2 displayed strong positive correlations with each other, and presented medium-strong negative correlations with Fs and WD. Further analysis of previous sampling periods revealed similar iterations of the results observed from the June 2018 data, as demonstrated in Supporting Information Tables S2 to S5. A weak to moderate correlation between pollutant concentration and distance from the emission source (RT) was observed throughout the study.

Bivariate analysis of SO_2 and pSO_4^{2-} revealed an insignificant relationship between pollutants over the full study period (R^2= 0.20), as shown in Fig. 8. Further comparison of filter-pack measured SO_2 and pSO_4^{2-} from individual sampling periods resulted in minor improvements in correlation strength (campaign four: R^2 = 0.40, three: R^2 = 0.36, two: R^2 = 0.07, and one: R^2 = 0.37); high SO_2 measurements introduced unpredictable scattering. Fig. 9 Illustrates that comparison of SO_2 and corresponding estimated F_s values produced a comparatively stronger trend with notably reduced variation throughout the study period. Given that the dependant variable, F_s referenced the independent variable, SO_2, curve fitting (rather than linear regression) analysis was employed to illustrate the visible trend between data-points. In order to produce a

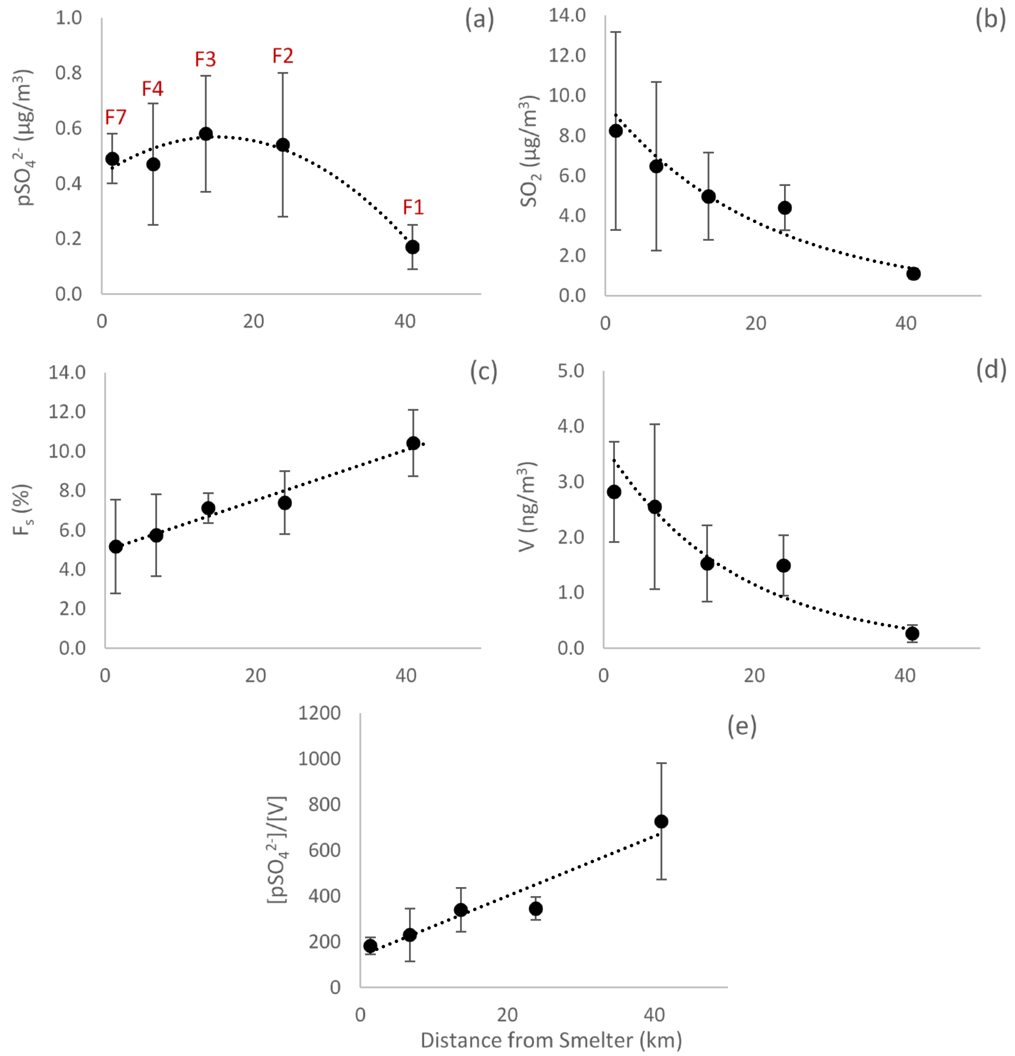

Fig. 6. Filter-pack measured (a) pSO_4^{2-} ($\mu g\ m^{-3}$), (b) F_s (%), (c) SO_2 ($\mu g\ m^{-3}$), (d) V ($ng\ m^{-3}$), and (e) $[pSO_4^{2-}]/[V]$ ratio during the June–July 2018 sampling period plotted against site distance (km) from the Rio Tinto smelting facility. Sites situated within the northern section of the RT emission plume (F1, F2, F3, F4, and F7) are displayed and labelled in plot "a". The curve of best fit has been presented for each plot. Positive and negative error bars indicate ± 1 standard deviation for each sampling location.

linear curve of best fit, SO_2 and F_s data were independently natural-log (LN) transformed, as displayed in Fig. 9.

3.5 SO_2 Passive Sampler Observations

As shown in Table S6 in Supporting Information, average ambient SO_2 measured during the June–October sampling periods of both 2017 and 2018 were 5.49 and 5.98 $\mu g\ m^{-3}$, respectively. Site averages ranged from 0.90 (Lakelse) to 12.90 $\mu g\ m^{-3}$ (Haul Road) during the first period, and 0.94 (Lakelse) to 13.93 $\mu g\ m^{-3}$ (V11) during the second. Average SO_2 followed a negative spatial gradient relative to distance from the smelting facility during both 2017 and 2018 exposure periods. As displayed in Fig. 10, the observed trend was non-linear (negative-exponential), as the rate of SO_2 decline was steepest between samplers deployed in close-proximity to the smelter.

3.6 pSO_4^{2-} Spatial/Temporal Variability

Average F_s ratios (extrapolated from the IVL SO_2 data) followed a significant positive-linear rate of increase relative to distance downwind of the RT facility. Predicted average F_s appeared to

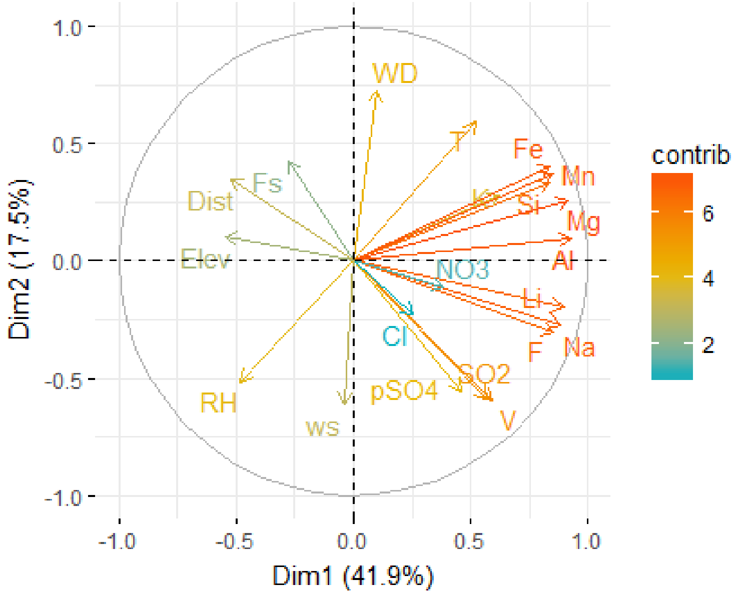

Fig. 7. Principal component analysis (PCA) evaluating underlying variability of the combined dataset (containing filter-pack, meteorological, and physical variables) observed during the fourth sampling campaign. Principal components one (representing 41.9% of explained variance) and two (17.5% of explained variance) are plotted. Variable contribution (%) to principal components variation is presented for each eigenvector, refer to legend titled "contrib" for scale.

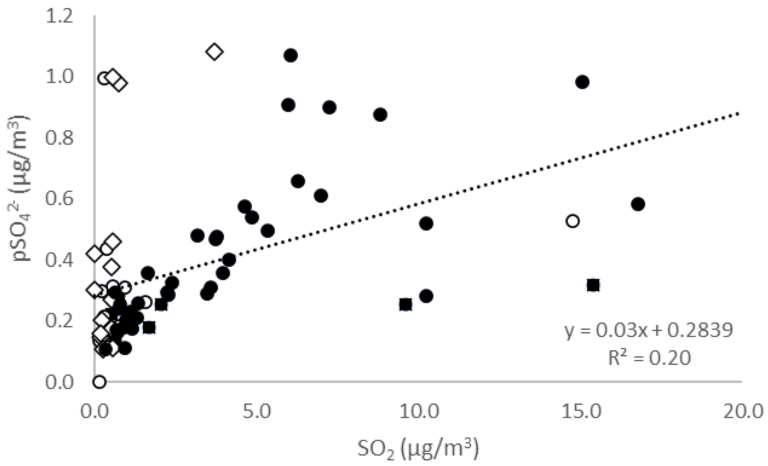

Fig. 8. Comparison of filter-pack measured SO_2 ($\mu g\ m^{-3}$) and pSO_4^{2-} ($\mu g\ m^{-3}$) throughout sampling campaigns one through four. Shaped data-points indicate individual sampling periods, where the black squares, hollow circles, hollow diamonds, and black circles represent periods one through four, respectively. The line of best fit (black line) with corresponding regression equation and coefficient of determination are displayed.

increase at a rate of 2.4 and 2.5% km^{-1} (with distance from the smelter, along the plume's central transect) during the June–October 2017 and 2018 sampling periods, respectively, as shown in Fig. 11.

Average predicted pSO_4^{2-} during the June–November 2017 IVL exposure ranged 0.24 (Lakelse station) to 0.69 $\mu g\ m^{-3}$ (Haul Rd.), and 0.23 (Lakelse) to 0.77 $\mu g\ m^{-3}$ (Haul Road) during the June–Sept 2018 IVL exposure. Estimated pSO_4^{2-} concentrations decreased relative to distance from the smelter (owing to the observed decline in corresponding SO_2 concentrations) during all observational periods, as displayed in Fig. S4.

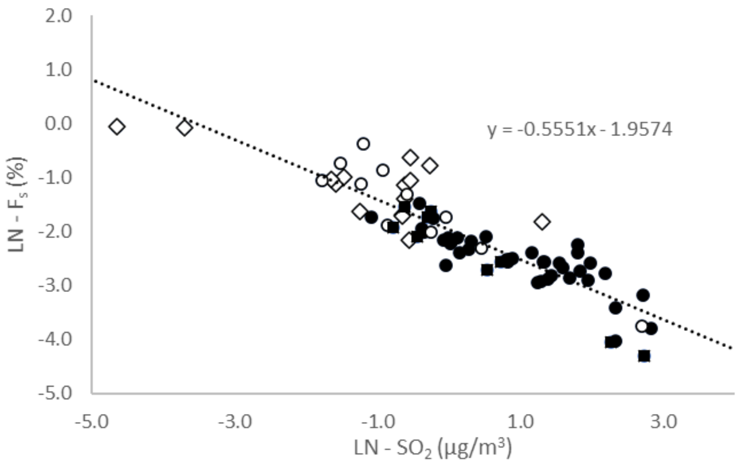

Fig. 9. Comparison of natural-log transformed SO_2 (μg m^{-3}) and F_s (%) measured via filter-pack sampler during sampling campaigns one through four. Shaped data-points indicate individual sampling periods, where black squares, hollow circles, hollow diamonds, and black circles represent sampling periods one through four, respectively. The line of best fit (black line) and corresponding linear equation is displayed.

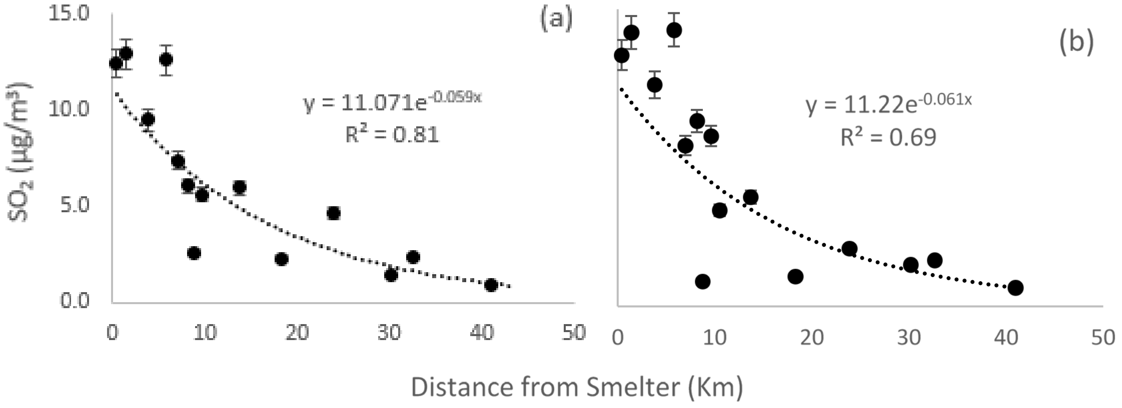

Fig. 10. Average SO_2 (μg m^{-3}) measured by IVL samplers situated within the RT smelter emission plume during the (a) June–October 2017 and (b) June–October 2018 exposure periods plotted against the corresponding site distance (km) from the smelting facility. The line of best fit with corresponding equation and coefficient of determination (R^2), in addition to positive and negative error bars representing sampler variation (± replicate CV) are displayed.

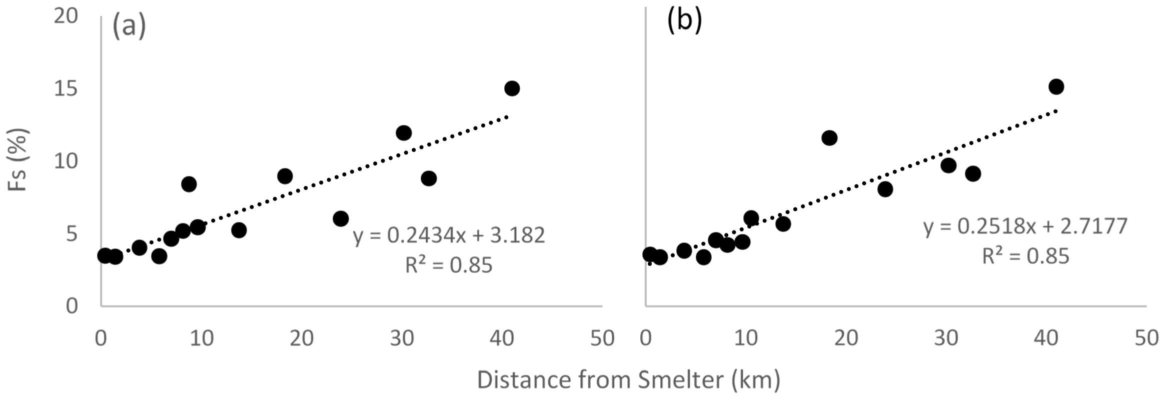

Fig. 11. Extrapolated F_s (%) at select IVL passive sampling locations during (a) June–October 2017 and (b) July–October 2018 plotted against site (linear) distance (km) from the Rio Tinto smelting facility. The line of best fit with corresponding equation and coefficient of determination (R^2) are displayed.

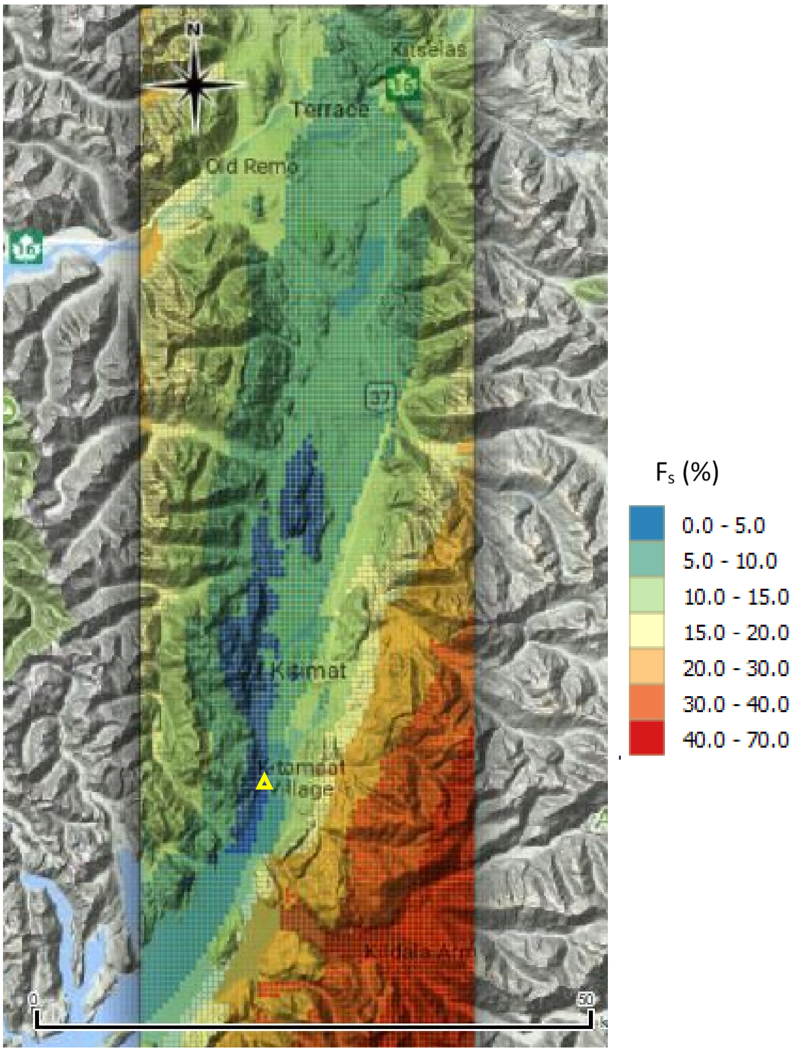

Fig. 12. Extrapolated annual average F_s (%) throughout the Kitimat Valley based on CALPUFF modelled (post-KMP) annual average SO_2 ($\mu g\ m^{-3}$) (ESSA Technologies Ltd., 2013). The location of the RT smelting facility is indicated by the yellow triangle.

The F_s ratios extrapolated from the annual CALPUFF SO_2 estimates were observed at their lowest within the smelter's plume, where (owing to declining SO_2) F_s gradually increased relative to distance from the emission source, as seen in Fig. 12. Estimated F_s within the broader RT plume (the modelled region experiencing $> 1\ \mu g\ m^{-3}$ SO_2, post-KMP) was predicted to range between 2.2–14.2%, with an average value of 9.2%. It should be noted that F_s and resulting pSO_4^{2-} values extrapolated from the CALPUFF annual average SO_2 did not account for uncertainty in the model simulations, including the limited meteorological years (2006, 2008, and 2009). Nonetheless. modelled SO_2 followed the same spatial pattern observed in the filter-packs, and the extrapolated data provide an estimated of the spatial variability of F_s within the valley.

4 DISCUSSION

4.1 Characterization of the RT Emission Plume

Comparison of gaseous and particulate species measured via filter-pack samplers revealed two principal component groupings during the summer 2017 and 2018 sampling periods. The first grouping (denoted by PC1) presented a strong positive correlation with elements associated with crustal emissions (Si, Mg, Fe, Mn) and was assumed to be partially representative of dust emissions (Gunawardana *et al.*, 2012) from active unpaved regions within or surrounding the RT facility. The second variable grouping characterized by positively correlated SO_2, pSO_4^{2-}, and V represented smelter emissions. The known association of these pollutants with the Al smelting process, and the positive correlation between species provided indirect evidence that the RT facility was the common emission source in the study region.

The observed peak in pSO_4^{2-} concentrations during the third campaign (February 16–23, 2018) may have been the result of atmospheric inversion events combined with elevated wood burning in residential areas north of the study region (Novakov *et al.*, 1974; Mamane and Gottlieb, 1989; Buzcu *et al.*, 2006). Predominant northerly winds during this period likely transported these polluted air masses toward Kitimat.

Decreasing concentrations of SO_x and V northward along the valley transect suggested a continuous removal/diffusion of the pollutant species following initial emission from the RT facility. The non-linear rate of SO_2 decline (measured by the IVL network) relative to distance from the smelter was likely a product of combined removal mechanisms (SO_x oxidization, dilution, and (wet and dry) deposition), which are known to contribute to a rapid reduction of SO_2 within the earlier stages of point-source emission plumes (Springston *et al.*, 2005; Zhou *et al.*, 2011).

4.2 pSO_4^{2-} and F_s

Insignificant correlations between filter-pack measured SO_2 and pSO_4^{2-} failed to indicate whether aerosol formation within the Kitmat Valley was SO_2-limited, thus SO_2 could not serve as a predictor of pSO_4^{2-} concentrations. Previous field measurements of in-plume oxidation processes have indicated that SO_2 and pSO_4^{2-} exhibit a non-linear relationship (Luria *et al.*, 2001). However, such a relationship was not apparent among current filter-pack measurements, thus a linear fit was ascribed to the data.

Disagreement between SO_2 and secondary sulphate measurements was suspected to be the product of inter-seasonal variation, particularity between the summer and winter/autumn sampling periods. Previous studies, including those by Lusis and Wiebe (1976) and Chan *et al.* (1980) found that due to an abundance of SO_2 within early-stage emission plumes, SO_x oxidation is limited by the mixing-rate of reactive species (including OH radicals). The RT emission plume may possess similar reactive characteristics, as indicated by the weak correlation between SO_2 and pSO_4^{2-}.

The increasing pSO_4^{2-}/V values relative to distance from the RT smelter (along the central transect) strongly indicated that pSO_4^{2-} formation was occurring within the emission plume. Owing to the similar dry deposition rates experienced by particulate SO_4^{2-} and V (Hazi *et al.*, 2003; Sakata and Marumoto, 2004), preferential loss of individual species likely had a limited influence over ratio variation within the plume. The significant correlations observed between the pSO_4^{2-}/V ratio against sampler distance from smelter indicated a relative increase of pSO_4^{2-} following initial emission; these trends provided independent evidence indicating in-plume pSO_4^{2-} formation was occurring during the fourth sampling period.

Despite the gradual formation of SO_4^{2-} aerosols within the smelter's plume, filter-pack measured pSO_4^{2-} remained below an average of 0.1 µg S m^{-3} (excluding exposure 3 due to the inversion event), while average SO_2 ranged from 1.0 to 1.8 µg S m^{-3}. Estimated average F_s along the central plume transect was low, as filter-pack fractions infrequently exceeded 20% downwind of the smelter. As such, pSO_4^{2-} had a minor influence over total atmospheric SO_x within the primary plume transect. The comparatively high F_s in the regions east and west of the plume was indicative of a concentration gradient approaching background ambient SO_x fractions. Owing to its longer atmospheric residence time (Hains *et al.*, 2008; Lee *et al.*, 2011), the relative concentration of pSO_4^{2-} will likely exceed that of SO_2 in the absence of primary emissions.

5 CONCLUSIONS

Between June 2017 to October 2018, active filter-pack and passive-diffusive sampling networks were established throughout the Kitimat Valley with the objective to evaluate the spatial and temporal variation of pSO_4^{2-} and SO_2 downwind of the RT aluminium smelting facility, which was recently permitted to emit SO_2 at a maximum rate of 42 t d^{-1}. Filter-pack observations along the northern plume transect confirmed that the concentration of pSO_4^{2-} relative to total SO_x increased downwind of the emission source, while increasing pSO_4^{2-}/V spatial gradients indicated in-plume secondary-sulphate formation occurred. Filter-pack measured SO_2 was not significantly correlated with pSO_4^{2-} throughout the Valley. However, filter-pack measurements suggested that secondary-sulphate did not significantly contribute to total atmospheric SO_x within the RT emission plume (field campaign average $F_s < 20\%$; $pSO_4^{2-} < 0.1\ \mu g\ S\ m^{-3}$; $SO_2 > 1.0\ \mu g\ S\ m^{-3}$). The filter-pack network proved to be a versatile and cost-effective approach to evaluating SO_x variation downwind of the RT smelter, likely attributable to the plume's spatial consistency throughout the Kitimat Valley and the limited influence from additional pollutant species in this background (pristine) region.

ACKNOWLEDGMENTS

The study was made possible through logistical support and funding provided by Rio Tinto and support from the NSERC CREATE program. We gratefully thank Kevin Adkinson (laboratory manager) and the field assistants from Trent University and University College Dublin for their assistance during sampling and analysis.

SUPPLEMENTARY MATERIAL

Supplementary data associated with this article can be found in the online version at https://doi.org/10.4209/aaqr.200528

REFERENCES

Arends, B., Baard, J., Ten Brink, H. (1997). Trends in summer sulphate in Europe. Atmos. Environ. 31, 4063–4072. https://doi.org/10.1016/s1352-2310(97)00283-5

Blanchard, D., Aherne, J. (2019). Spatiotemporal variation in summer ground-level ozone in the Sandbanks Provincial Park, Ontario. Atmos. Pollut. Res. 10, 931–940. https://doi.org/10.1016/j.apr.2019.01.001

Bunce, N. (1998). Environmental Chemistry. Wuerz Publishing Winnipeg, Canada.

Buzcu, B., Yue, Z., Fraser, M., Nopmongcol, U., Allen, D. (2006). Secondary particle formation and evidence of heterogeneous chemistry during a wood smoke episode in Texas. J. Geophys. Res. 111, D10S13. https://doi.org/10.1029/2005jd006143

Carmichael, G., Ferm, M., Adikary, S., Ahmad, J., Mohan, M., Hong, M., Chen, L., Fook, L., Liu, C. M., Soedomo, M., Tran, G., Suksomsank, K., Zhao, D., Arndt, R., Chen, L.L. (1995). Observed regional distribution of sulfur dioxide in Asia. Water Air Soil Pollut. 85, 2289–2294. https://doi.org/10.1007/bf01186175

Carmichael, G.R., Ferm, M., Thongboonchoo, N., Woo, J.H., Chan, L.Y., Murano, K., Viet, P.H., Mossberg, C., Bala, R., Boonjawat, J., Upatum, P., Mohan, M., Adhikary, S.P., Shrestha, A.B., Pienaar, J.J., Brunke, E.B., Chen, T., Jie, T., Guoan, D., Peng, L.C., *et al.* (2003). Measurements of sulfur dioxide, ozone and ammonia concentrations in Asia, Africa, and South America using passive samplers. Atmos. Environ. 37, 1293–1308. https://doi.org/10.1016/S1352-2310(02)01009-9

Chan, W., Vet, R., Lusis, M., Hunt, J., Stevens, R. (1980). Airborne sulfur dioxide to sulfate oxidation studies of the INCO 381M chimney plume. Atmos. Environ. 14, 1159–1170. https://doi.org/10.1016/0004-6981(80)90180-8

Clague, J. (1985). Deglaciation of the Prince Rupert e Kitimat area, British Columbia. Can. J. Earth Sci. 22, 256–265. https://doi.org/10.1139/e 85-022

Clague, J. (1994). Quaternary Geology and Geomorphology, Smithers–Terrace–Prince Rupert Area, British Columbia. Geological Survey of Canada, Memoir No. 413. 71p.

Cowden, P., Aherne, J. (2019). Assessment of atmospheric metal deposition by moss biomonitoring in a region under the influence of a long standing active aluminium smelter. Atmos. Environ. 201, 84–91. https://doi.org/10.1016/j.atmosenv.2018.12.022

Davidson, C., Phalen, R., Solomon, P. (2005). Airborne particulate matter and human health: A review. Aerosol Sci. Technol. 39, 737–749. https://doi.org/10.1080/02786820500191348

EANET (2003). Technical Document for Filter Pack Methods in East Asia. The Third Session of the

Science Advisory Committee. Acid Deposition Monitoring Network in East Asia. Pattaya, Thailand. http://www.eanet.asia/product/technical_document/techdoc_fp.pdf

Edwards, L. (2014). The history and future challenges of calcined petroleum coke production and use in aluminum smelting. JOM 67, 308–321. https://doi.org/10.1007/s11837-014-1248-9

Environment and Climate Change Canada (2017). Historical Data. Government of Canada. Retrieved September 16, 2016. http://climate.weather.gc.ca/climate_normals/results_1981_2010_e.html?stnID=402&dCode=&dispBack=1

Espinosa, A., Ternero Rodríguez, M., Barragán de la Rosa, F., Jiménez Sánchez, J. (2001). Size distribution of metals in urban aerosols in Seville (Spain). Atmos. Environ. 35, 2595–2601. https://doi.org/10.1016/s1352-2310(00)00403-9

ESSA Technologies Ltd. (2013). Sulphur Dioxide Technical Assessment Report in Support of the 2013 Application to Amend the P2-00001 Multimedia Permit for the Kitimat Modernization Project. Volume 2: Final Technical Report. Prepared for Rio Tinto Alcan, Kitimat, B.C. 450 pp.

European Monitoring and Evaluation Programme (EMEP) (2001). EMEP manual for sampling and chemical analysis. European Monitoring and Evaluation Programme. EMEP/CCC-Report 1/95. https://projects.nilu.no//ccc/manual/index.html

Ferm, M., Rodhe, H. (1997). Measurements of air concentrations of SO_2, NO_2 and NH_3 at rural and remote sites in Asia. J. Atmos. Chem. 27, 17–29. https://doi.org/10.1023/A:1005816621522

Ferm, M., Svanberg, P. (1998). Cost-efficient techniques for urban- and background measurements of SO_2 and NO_2. Atmos. Environ. 32, 1377–1381. https://doi.org/10.1016/s1352-2310(97)00170-2

Friedlander, S. (1978). A review of the dynamics of sulfate containing aerosols. Atmos. Environ. 12, 187–195. https://doi.org/10.1016/0004-6981(78)90200-7

Gillani, N., Kohli, S., Wilson, W. (1981). Gas-to-particle conversion of sulfur in power plant plumes—I. Parametrization of the conversion rate for dry, moderately polluted ambient conditions. Atmos. Environ. 15, 2293–2313. https://doi.org/10.1016/0004-6981(81)90261-4

Gorham, E. (1955). On the acidity and salinity of rain. Geochim. Cosmochim. Acta 7, 231–239. https://doi.org/10.1016/0016-7037(55)90034-x

Grosjean, D., Friedlander, S. (1975). Gas-particle distribution factors for organic and other pollutants in the Los Angeles atmosphere. J. Air Pollut. Control Assoc. 25, 1038–1044. https://doi.org/10.1080/00022470.1975.10470176

Gunawardana, C., Goonetilleke, A., Egodawatta, P., Dawes, L., Kokot, S. (2012). Source characterisation of road dust based on chemical and mineralogical composition. Chemosphere 87, 163–170. https://doi.org/10.1016/j.chemosphere.2011.12.012

Hains, J., Taubman, B., Thompson, A., Stehr, J., Marufu, L., Doddridge, B., Dickerson, R. (2008). Origins of chemical pollution derived from Mid-Atlantic aircraft profiles using a clustering technique. Atmos. Environ. 42, 1727–1741. https://doi.org/10.1016/j.atmosenv.2007.11.052

Hand, J., Schichtel, B., Pitchford, M., Malm, W., Frank, N. (2012). Seasonal composition of remote and urban fine particulate matter in the United States. J. Geophys. Res. 117, D05209. https://doi.org/10.1029/2011jd017122

Hazi, Y., Heikkinen, M., Cohen, B. (2003). Size distribution of acidic sulfate ions in fine ambient particulate matter and assessment of source region effect. Atmos. Environ. 37, 5403–5413. https://doi.org/10.1016/j.atmosenv.2003.08.034

Hewitt, C. (2001). The Atmospheric chemistry of sulphur and nitrogen in power station plumes. Atmos. Environ. 35, 1155–1170. https://doi.org/10.1016/s1352-2310(00)00463-5

Huntzicker, J., Hoffman, R., Cary, R. (1984). Aerosol sulfur episodes in St. Louis, Missouri. Environ. Sci. Technol. 18, 962–967. https://doi.org/10.1021/es00130a012

Husar, J.D., Husar, R.B., Macias, E.S., Wilson, W.E., Durham, J.L., Shepherd, W.K., Anderson, J.A. (1976). Particulate sulfur analysis: Application to high time resolution aircraft sampling in plumes. Atmos. Environ. 10, 591–595. https://doi.org/10.1016/0004-6981(76)90043-3

Jha, G., Cannova, F., Sadler, B. (2016). Increasing Coke Impurities — Is this Really a Problem for Metal Quality? in: Suarez, C.E. (Ed.), Light Metals 2012, Springer International Publishing, Cham, pp. 1303–1306. https://doi.org/10.1007/978-3-319-48179-1_225

Kadowaki, S. (1986). On the nature of atmospheric oxidation processes of sulfur dioxide to sulfate and of nitrogen dioxide to nitrate on the basis of diurnal variations of sulfate, nitrate, and other pollutants in an urban area. Environ. Sci. Technol. 20, 1249–1253. https://doi.org/10.1021/es00154a009

Khoder, M. (2002). Atmospheric conversion of sulfur dioxide to particulate sulfate and nitrogen dioxide to particulate nitrate and gaseous nitric acid in an urban area. Chemosphere 49, 675–684. https://doi.org/10.1016/S0045-6535(02)00391-0

Lee, L.A., Carslaw, K.S., Pringle, K.J., Mann, G.W., Spracklen, D.V. (2011). Emulation of a complex global aerosol model to quantify sensitivity to uncertain parameters. Atmos. Chem. Phys. 11, 12253–12273. https://doi.org/10.5194/acp-11-12253-2011

Luria, M., Imhoff, R., Valente, R., Parkhurst, W., Tanner, R. (2001). Rates of conversion of sulfur dioxide to sulfate in a scrubbed power plant plume. J. Air Waste Manage. Assoc. 51, 1408–1413. https://doi.org/10.1080/10473289.2001.10464368

Lusis, M., Wiebe, H. (1976). The rate of oxidation of sulfur dioxide in the plume of a nickel smelter stack. Atmos. Environ. 10, 793–798. https://doi.org/10.1016/0004-6981(76)90133-5

Mamane, Y., Gottlieb, J. (1989). The study of heterogeneous reactions of carbonaceous particles with sulfur and nitrogen oxides using a single particle approach. J. Aerosol Sci. 20, 575–584. https://doi.org/10.1016/0021-8502(89)90104-3

Margitan, J. (1984). Mechanism of the atmospheric oxidation of sulfur dioxide. Catalysis by hydroxyl radicals. J. Phys. Chem. 88, 3314–3318. https://doi.org/10.1021/j150659a035

Millero, F. (1974). The physical chemistry of seawater. Annu. Rev. Earth Planet. Sci. 2, 101–150. https://doi.org/10.1146/annurev.ea.02.050174.000533

Mohnen, V. (1988). The challenge of acid rain. Sci. Am. 259, 30–38. https://doi.org/10.1038/scientificamerican0888-30

Nicholson, K., Davies, T. (1987). Field measurements of the dry deposition of particulate sulphate. Atmos. Environ. 21, 1561–1571. https://doi.org/10.1016/0004-6981(87)90318-0

Novakov, T., Chang, S., Harker, A. (1974). Sulfates as pollution particulates: Catalytic formation on carbon (Soot) particles. Science 186, 259–261. https://doi.org/10.1126/science.186.4160.259

Nriagu, J. (1998). Vanadium in the Environment. Wiley, New York.

Parungo, F., Nagamoto, C., Maddl, R. (1987). A study of the mechanisms of acid rain formation. J. Atmos. Sci. 44, 3162–3174. https://doi.org/10.1175/1520-0469(1987)044%3C3162:ASOTMO%3E2.0.CO;2

Roberts, D., Williams, D. (1979). The kinetics of oxidation of sulphur dioxide within the plume from a sulphide smelter in a remote region. Atmos. Environ. 13, 1485–1499. https://doi.org/10.1016/0004-6981(79)90057-x

Sakata, M., Marumoto, K. (2004). Dry deposition fluxes and deposition velocities of trace metals in the Tokyo metropolitan area measured with a water surface sampler. Environ. Sci. Technol. 38, 2190–2197. https://doi.org/10.1021/es030467k

Schlesinger, W., Klein, E., Vengosh, A. (2017). Global biogeochemical cycle of vanadium. PNAS 114, E11092–E11100. https://doi.org/10.1073/pnas.1715500114

Singh, M., Jaques, P., Sioutas, C. (2002). Size distribution and diurnal characteristics of particle-bound metals in source and receptor sites of the Los Angeles Basin. Atmos. Environ. 36, 1675–1689. https://doi.org/10.1016/s1352-2310(02)00166-8

Solomon, S., Qin, D., Manning, M., Chen, Z., Marquis, M., Averyt, K.B., Tignor, M., Miller, H.L. (2007). Climate Change 2007: The Physical Science Basis. Contribution of Working Group I to the Fourth Assessment Report of the Intergovernmental Panel on Climate Change, Cambridge Univ. Press, New York, p. 108.

Springston, S., Kleinman, L., Brechtel, F., Lee, Y., Nunnermacker, L., Wang, J. (2005). Chemical evolution of an isolated power plant plume during the Texas 2000 Study. Atmos. Environ. 39, 3431–3443. https://doi.org/10.1016/j.atmosenv.2005.01.060

Swaans, W., Goelen, E., De Fré, R., Damen, E., Van Avermaet, P., Roekens, E., Keppens, V. (2007). Laboratory and field validation of a combined NO_2–SO_2 Radiello passive sampler. J. Environ. Monit. 9, 1231–1240. https://doi.org/10.1039/B708925B

Van Reeuwijk, H., Fischer, P., Harssema, H., Briggs, D., Smallbone, K., Lebret, E. (1998). Field comparison of two NO_2 passive samplers to assess spatial variation. Environ. Monit. Assess. 50, 37–51. https://doi.org/10.1023/A:1005703722232

Watanabe, M., Takamatsu, T., Koshikawa, M., Sakamoto, K., Inubushi, K. (2006). Simultaneous determination of atmospheric sulfur and nitrogen oxides using a battery-operated portable filter pack sampler. J. Environ. Monit. 8, 167–173. https://doi.org/10.1039/b512217a

Wigley, T. (1989). Possible climate change due to SO_2-derived cloud condensation nuclei. Nature

339, 365–367. https://doi.org/10.1038/339365a0

Williston, P., Aherne, J., Watmough, S., Marmorek, D., Hall, A., de la Cueva Bueno, P., Murray, C. Henolson, A., Laurence, J. (2016). Critical levels and loads and the regulation of industrial emission in northwest British Columbia, Canada. Atmos. Environ. 146, 311–323. https://doi.org/10.1016/j.atmosenv.2016.08.058

Zbieranowski, A.L., Aherne, J. (2012). Ambient concentrations of atmospheric ammonia, nitrogen dioxide and nitric acid across a rural–urban–agricultural transect in Southern Ontario, Canada. Atmos. Environ. 62, 481–491. https://doi.org/10.1016/j.atmosenv.2012.08.040

Zhang, X., Li, F., Zhang, L., Zhao, Z., Norback, D. (2014). A longitudinal study of sick building syndrome (SBS) among pupils in relation to SO_2, NO_2, O_3 and PM_{10} in schools in China. PLoS One 9, e112933. https://doi.org/10.1371/journal.pone.0112933

Zhou, W., Cohan, D.S., Pinder, R.W., Neuman, J.A., Holloway, J.S., Peischl, J., Ryerson, T.B., Nowak, J.B., Flocke, F., Zheng, W.G. (2012). Observation and modeling of the evolution of Texas power plant plumes. Atmos. Chem. Phys. 12, 455–468. https://doi.org/10.5194/acp-12-455-2012